Autonomous Recharging and Flight Mission Planning for Battery-operated Autonomous Drones

CHIEN-MING TSENG, Masdar Institute CHI-KIN CHAU, Masdar Institute KHALED ELBASSIONI, Masdar Institute MAJID KHONJI, Masdar Institute

Autonomous drones (also known as unmanned aerial vehicles) are increasingly popular for diverse applications of light-weight delivery and as substitutions of manned operations in remote locations. The computing systems for drones are becoming a new venue for research in cyber-physical systems. Autonomous drones require integrated intelligent decision systems to control and manage their flight missions in the absence of human operators. One of the most crucial aspects of drone mission control and management is related to the optimization of battery lifetime. Typical drones are powered by on-board batteries, with limited capacity. But drones are expected to carry out long missions. Thus, a fully automated management system that can optimize the operations of battery-operated autonomous drones to extend their operation time is highly desirable. This paper presents several contributions to automated management systems for battery-operated drones: (1) We conduct empirical studies to model the battery performance of drones, considering various flight scenarios. (2) We study a joint problem of flight mission planning and recharging optimization for drones with an objective to complete a tour mission for a set of sites of interest in the shortest time. This problem captures diverse applications of delivery and remote operations by drones. (3) We present algorithms for solving the problem of flight mission planning and recharging optimization. We implemented our algorithms in a drone management system, which supports real-time flight path tracking and re-computation in dynamic environments. We evaluated the results of our algorithms using data from empirical studies. (4) To allow fully autonomous recharging of drones, we also develop a robotic charging system prototype that can recharge drones autonomously by our drone management system. Overall, we present a comprehensive study on flight mission planning of battery-operated autonomous drones, considering autonomous recharging.

CCS Concepts: •Computer systems organization \rightarrow Embedded and cyber-physical systems; •Computing methodologies \rightarrow Robotic planning; •Theory of computation \rightarrow Dynamic graph algorithms;

Additional Key Words and Phrases: Autonomous Drones, Flight Mission Planning, Recharging Optimization, Automated Drone Management

ACM Reference format:

1 INTRODUCTION

Aerial vehicles are becoming a novel means of logistics. Often referred as drones in popular terminology, or unmanned aerial vehicles in technical terminology, they have several advantages

Permission to make digital or hard copies of all or part of this work for personal or classroom use is granted without fee provided that copies are not made or distributed for profit or commercial advantage and that copies bear this notice and the full citation on the first page. Copyrights for components of this work owned by others than ACM must be honored. Abstracting with credit is permitted. To copy otherwise, or republish, to post on servers or to redistribute to lists, requires prior specific permission and/or a fee. Request permissions from permissions@acm.org.

© 2017 ACM. XXXX-XXXX/2017/1-ART1 \$15.00

DOI: xx.xxxx/xxxxxxx.xxxxxxx

over ground based transportations. (1) *Agility*: There is little restriction in the sky, unlike on the ground with obstacles. Drones can travel across space in straight paths. They are usually small in size, with nimble navigating ability. (2) *Swiftness*: Aerial transportation is usually not hampered by traffic congestions. The time to arrival is mostly reflected by the travelled distance. Drones can also be rapidly launched by catapults, and drop off payloads by parachutes with short response time. (3) *Energy-efficiency*: Drones are typically light-weight, which consume less energy. They are particularly energy-efficient for transporting light-weight items in short trips, whereas ground vehicles are useful for carrying heavier objects in long distance. (4) *Safeness*: There is no on-board human operator or driver. Drones can keep a safe distance from human users. Unmanned transportation missions are specially desirable in hazardous environments.

These advantages of drones enable diverse applications for light-weight goods transportation and as substitutions of manned operations in remote locations. There are several notable applications of drones. (1) *Remote Surveillance*: Aerial transportation can access far-away remote regions, and geographically dispersed offshore locations. Particularly, oil and gas companies and utility providers, which rely on extensive surveillance, measurements, mapping and surveying, maintenance operations for dispersed facilities, will be major users of drones. (2) *Search and Rescue*: Drones can be deployed in ad hoc manner. In emergency with damaged or unreliable infrastructure, drones can overcome the difficulty of accessing in isolated regions, enabling fast transportation with great convenience and flexibility. (3) *Hazardous Missions*: Drones are excellent solutions for unmanned missions in risky or hazardous areas, in particular, for taking measurements in high-altitude, or bio/chemical harmful environments. Human supervisors can remotely control the drones to carry out dangerous operations. (4) *Light-weight Items Delivery*: Parcels, medical items, and mail require speedy delivery. Drones are effective in solving the last-leg problem of the distribution chain from depots to homes of end-users. A recent study by Amazon [13] reports that 44% of the US population are within 20 miles from its depot facility. Hence, it is practical to employ drones for delivery.

Therefore, in the near future, fully autonomous drones are expected for extensive deployment, giving rise to a new class of intelligent systems for logistics. Hence, the computing systems for drones are becoming an exciting new venue for research in cyber-physical systems. Autonomous drones require integrated intelligent decision systems to control and manage their flight missions in the absence of human operators. Despite increasingly popular applications of drones in diverse sectors, the operations of drones are plagued with several challenges:

- Limited Battery Lifetime: Typical drones are electric vehicles, powered by on-board batteries. Hence, the performance of drones is critically constrained by limited battery lifetime. Many drones are only suitable for short-range trips, which considerably limit their applicability. To optimize the battery performance of drones, there requires an intelligent management system to track the real-time state-of-charge, and optimize the operations accordingly.
- Dynamic Operating Environments: Drones are expected to travel in certain high altitude, and hence are significantly susceptible by wind and weather conditions. These conditions are highly dynamic, and should be accounted for in a real-time manner. Also, drones are light-weight, and the impact by wind is even more substantial. Drone management system should take explicit consideration of the dynamic uncertain operating environments.

These challenges present unique problems for battery-operated autonomous drones. Since drones are expected to carry out long missions in dynamic environments, a fully automated management system that can optimize the operations of battery-operated autonomous drones to extend their operation time is highly desirable.

1.1 Our Contributions

To improve the practical usefulness of autonomous drones, this paper presents several contributions to automated management systems for battery-operated drones:

- (1) We conduct empirical studies to model the power consumption of drones, considering various flight scenarios. Accurate model of battery performance in different scenarios allows further flight mission planning and recharging optimization for drones.
- (2) We study a joint problem of flight mission planning and recharging optimization for drones, using the calibrated power consumption model of a drone, with an objective to complete a tour mission for a set of sites of interest in the shortest time. We also consider uncertainty in dynamic environments, such as wind conditions. This problem captures diverse applications of delivery and remote operations by drones.
- (3) We present algorithms for solving the problem of flight mission planning and recharging optimization. We implemented our algorithms in a drone management system, which supports real-time flight path tracking and re-computation in dynamic environments. We evaluated the results of our algorithms using data from empirical studies.
- (4) To allow fully autonomous recharging of drones, we also develop a robotic charging station prototype that can recharge drones autonomously by our drone management system. Autonomous recharging can significantly extend the battery lifetime of drones for longdistance missions.

2 RELATED WORK

There are diverse applications for drones, including delivery (e.g., for light-weight parcels, medical items, mail) and remote operations (e.g., wildlife surveillance, environmental surveying, search and rescue operations). Drones had been often studied for their flight and landing control mechanisms. For example, see the books [18, 19] for a good overview of the recent results. There are two aspects of literature about drones: 1) low-level transient control of flight operations, for example, controlling propellers and balance using PID controllers [3, 4], and 2) high-level planning and management of drone missions, for example, obstacle avoidance, localization and mapping and path planning [20]. However, the high-level studies typically focus on a single short-distance flight paths. Long-distance flight mission planning involving multiple trips and recharging optimization has been considered to a lesser extent, to the best of our knowledge. Moreover, there is a lack of prior work on flight mission optimization particularly considering battery-operated drones.

Most drones are aerial electric vehicles. The prior studies of logistic optimization mainly focus on ground electric vehicles, not on aerial electric vehicles. Nonetheless, drones exhibit different characteristics that create some unique challenges. For example, the impact of wind is more substantial for drone flight. In [12], graph signal sampling and recovery techniques are used to plan routes for autonomous aerial vehicles, and a method is proposed to plan an energy-efficient flight trajectory by considering the influences of wind. Further, there appears limited empirical studies of battery performance of drones, although the empirical studies of ground electric vehicles have been explored in the literature. Modelling and predicting electric vehicle power consumption has been the subject of a number of research papers. One method is the model-based whitebox approach, based on specific vehicle dynamics model to understand the consumption behavior of electric vehicles [16]. The power consumption estimation can also be obtained by a blackbox approach. For example, a general statistical approach using regression model, without vehicle dynamics model, can estimate the power consumption of vehicles [5]. Blackbox model is more tractable and more convenient for trip optimization. Hence, we will employ a similar blackbox model for aerial electric vehicles, but taking into account the flight conditions.

This work is related to the trip planning problem of electric vehicles [17]. There are recent results for path planning of electric vehicles considering recharging operations [6]. We adopt the solution proposed in [15] for the so-called tour gas station problem, for which efficient algorithms are designed for obtaining a near-optimal solution under certain assumptions. A variant of the classical algorithm [7] for the travelling salesman problem (TSP) was proposed in [15] for the tour gas station problem. In this work, we extend those methods to solve the problem for drone management by incorporating extensions to the settings of drone operations.

For fully autonomous drone management, drones should also be able to recharge themselves without manual intervention. Inductive charging for drones has been proposed that can flexibly recharge drones in an autonomous manner [2]. However, this work relies on a different solution, with a combination of a robotic arm that can accommodate drone recharging in arbitrary positions. To enable autonomous recharging of drones, an autonomous inductive charging system is initially proposed in [14], which is integrated with the management system of this paper.

3 EMPIRICAL STUDIES OF BATTERY PERFORMANCE OF DRONES

In order to accurately optimize the power consumption and flight missions of drones, we first conducted a series of empirical studies to determine the battery performance of drones, considering various flight scenarios. In particular, we evaluate the power consumption using two commercial drone models, 3DR Solo [1] and DJI Matrice 100 [8] (see Fig. 1 and their specifications in Table 1). Both drones support developer kits, which allow us to extract data and program the flight paths. After gathering sufficient measurement data, we can apply regression models to capture the power consumption behavior of the drones.



Fig. 1. Left: 3DR Solo. Right: DJI Matrice 100.

	3DR Solo	DJI Matrice 100		
Weight	2 kg	2.8 kg		
Dimensions	ensions $25 \text{cm} \times 46 \text{cm}$ $46 \text{cm} \times 46 \text{cm}$			
Battery	5200 mAh 14.8V	5700 mAh 22.8V		
Battery Weight	500 g	600 g		
Motors	880 kV (×4)	350 kV (×4)		
Max Speed	20 km/h	60 km/h		
Max Altitude	122 ft (FAA Regulation)	122 ft (FAA Regulation)		
Charging Duration	90 mins	180 mins		
Software	Python Developer Kit	DJI SDK & ROS		

Table 1. Specifications of 3DR Solo and DJI Matrice 100 drones.

3.1 Settings of Empirical Studies

A typical drone is equipped with a number of sensors for two main purposes: (1) for self-stabilizing the drone in the air, and (2) for remotely tracking the drone status (e.g., the battery state-of-charge (SoC)). The stability of a drone is controlled by three essential sensors (i.e., gyroscopes, accelerometers and barometers), with which it can maneuver itself in the air. The SoC is measured by the voltage and current sensors. A major part of power consumption of a drone is due to the powering of motors to lift itself in the air. Additional power consumption is required for the movements of the drone. The movements can be decomposed into vertical and horizontal directions. The barometer and GPS sensors can measure the 3-dimensional movements of a drone. The speed and position of a drone can be tracked by GPS and IMU modules, which also enable automatic navigation. The altitude of a drone can be tracked by barometer and GPS modules.

To understand the factors that determine the power consumption of a drone, we carried out the following experiments for obtaining empirical data in the rural areas, where the drone can fly in a straight path without obstacles:

- (1) *Impact of Motion*: The motions of a drone can be divided into three types: hovering, horizontal moving and vertical moving. We study the power consumption of a test drone in each motion type.
- (2) *Impact of Weight*: Typical drones can carry extra payloads, such as camera equipment or parcels. We study the impact of different weights of payloads attached to a test drone.
- (3) *Impact of Wind*: The major environmental factor that affects the drone is wind, including wind direction and speed. Wind may benefit the power consumption in some cases, as well as incurring resistance to the movement in other cases. We study the power consumption of a test drone in various wind conditions.

The experimental results are described as follows.

3.1.1 Impact of Motion. To study the power consumption of motions of a drone, we conducted three experiments. The battery power, barometer and GPS location, and speed data were collected in each experiment to analyze the performance of test drone 3DR Solo.

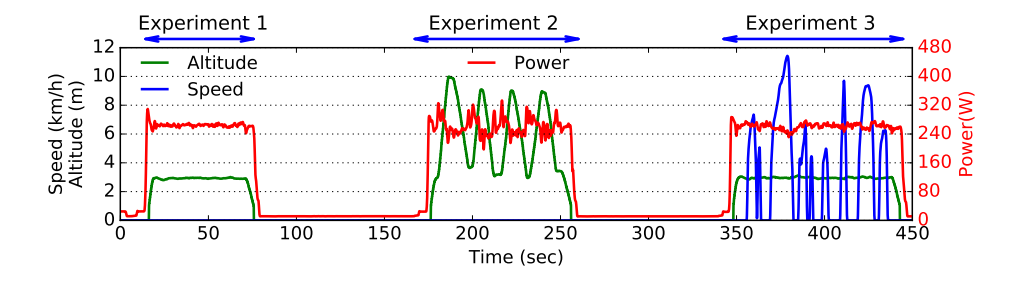


Fig. 2. Motion and battery power consumption of test drone 3DR Solo.

Fig. 2 depicts the recorded data traces of the three experiments of test drone 3DR Solo. We discuss several observations as follows:

• Experiment 1: The test drone hovered in the air without any movement in this experiment. Note that the drone may slightly drift around the takeoff location due to deviation error of GPS modules. We filter the speed data that is smaller than 0.5 m/s. This experiment shows the baseline power consumption of a flying drone. From the recorded data, we observe that the drone can maintain a sufficiently steady flying altitude with steady power consumption.

- Experiment 2: The test drone ascended and descended repeatedly in this experiment. The barometer data shows the altitude of the drone. The time series data allow us to compute the vertical acceleration and speed of the drone. We observe larger power fluctuations due to repeatedly vertical movements. Power consumption increases slightly, when the drone ascends steady.
- Experiment 3: The test drone moved horizontally without altering its altitude in this experiment. The GPS data comprises of speed and course angle of the drone. We also gathered average wind speed and direction using a wind speed meter during the experiment. We observe smaller power fluctuations due to horizontal movements. We also measure idle power consumption of the drone between the two experiments.
- 3.1.2 Impact of Weights. One of the practical purposes of drones is to deliver payloads, and hence, the total weight of a drone varies as the payload it carries. We carried out several experiments with different weights of payloads on the test drone 3DR Solo to obtain empirical data. Three different weights were tested on the drone. The drone was set to hover in the air without any movement to obtain the corresponding baseline power consumption.

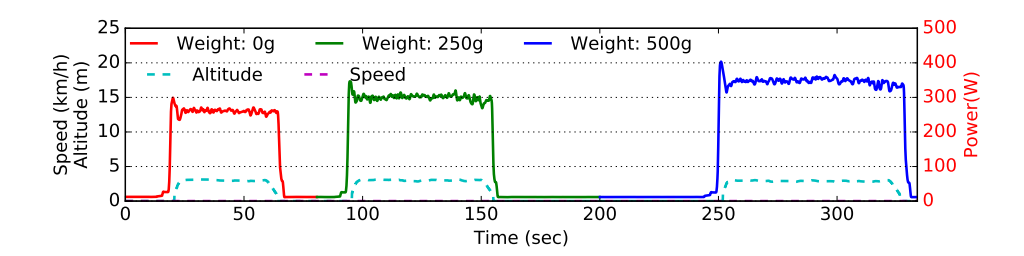


Fig. 3. Battery power consumption of test drone 3DR Solo with different payload weights.

Fig. 3 depicts the battery power consumption of the test drone carrying three different weights. We observe that power consumption increases almost linearly when the weight of payload increases. The weight limit of payload depends on the thrusts that the motors can produce. Note that the maximum payload weight is 500g for 3DR Solo.

3.1.3 Impact of Wind. Wind condition is a major environmental factor to affect the power consumption of test drone 3DR Solo. We conducted several experiments under different wind conditions: headwind by flying against the direction of wind, and tailwind by flying along the direction of wind. The experiments were carried out at the same location but on different days with different wind conditions. The wind directions and average speeds were measured using a wind speed meter for each experiment. Once the wind direction was determined, the drone was set to fly into a headwind or tailwind at maximum speed (18 km/h).

Fig. 4 depicts the battery power consumption of the drone under different wind conditions. We observe smaller power consumption when flying into headwind, which is due to the increasing thrust by *translational lift*, when the drone moves from hovering to forward flight. When flying into a headwind, translational lift increases due to the relative airflow over the propellers increases, resulting in less power consumption to hover the drone [11]. However, when the wind speed exceeds a certain limit, the aerodynamic drag may outweigh the benefit of translational lift. In our setting, the drone speed is relatively slow, even at maximum speed. Hence, flying into a headwind is likely more energy-efficient.

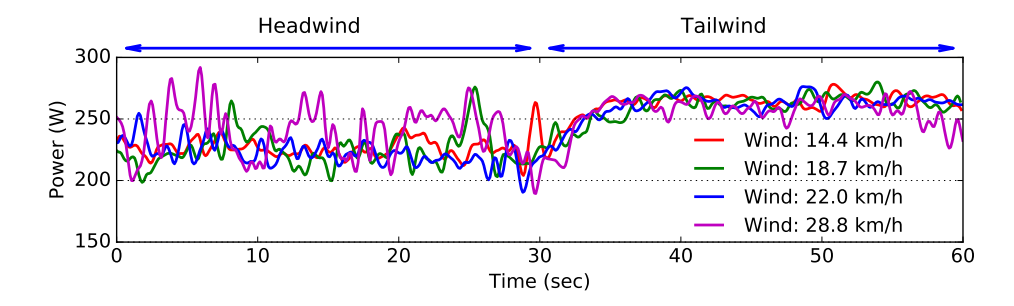


Fig. 4. Battery power consumption of test drone 3DR Solo under different wind conditions.

3.2 Regression Model of Power Consumption for Drone

Since drones are aerial electric vehicles, we can apply the methodology from the literature of general electric vehicles to model the power consumption of a drone. There are two main types of power consumption models of a drone:

- White-box Model: A straightforward approach is to employ a white-box microscopic behavior model for each drone that comprehensively characterizes the motor performance, aerodynamic environment, and battery systems. However, such a white-box model requires a large amount of data for calibration and detailed knowledge specific to a particular drone. For example, the aerodynamic parameters such as propeller efficiencies, motor efficiencies and drag coefficients are difficult to obtain accurately without resorting to sophisticated experimental setups like wind tunnel.
- Blackbox Model: A blackbox approach is more desirable, because it requires minimal
 knowledge of vehicle model with only a small set of measurable variables and parameters of
 the drone. In the subsequent sections, a blackbox model of power consumption of a drone
 will be utilized for flight mission planning and recharging optimization. The advantage of
 blackbox model is that it is obtained from simple data measurements without relying on
 sophisticated experimental setups.

This section describes a general multivariate blackbox model of power consumption for a drone that has been used extensively in the literature of electric vehicles [5, 9, 10, 21, 22], which will be verified in the later empirical studies.

Let the estimated battery power consumption of a drone be \hat{P} , which is estimated by a number of measurement parameters in the following linear equation:

$$\hat{P} = \begin{bmatrix} \beta_1 \\ \beta_2 \\ \beta_3 \end{bmatrix}^T \begin{bmatrix} \|\vec{v}_{xy}\| \\ \|\vec{a}_{xy}\| \\ \|\vec{v}_{xy}\| \|\vec{a}_{xy}\| \end{bmatrix} + \begin{bmatrix} \beta_4 \\ \beta_5 \end{bmatrix}^T \begin{bmatrix} \|\vec{v}_z\| \\ \|\vec{a}_z\| \\ \|\vec{v}_z\| \|\vec{a}_z\| \end{bmatrix} + \begin{bmatrix} \beta_7 \\ \beta_8 \\ \beta_9 \end{bmatrix}^T \begin{bmatrix} m \\ \vec{v}_{xy} \cdot \vec{w}_{xy} \end{bmatrix}$$
(1)

where

- \vec{v}_{xy} and \vec{a}_{xy} are the speed and acceleration vectors describing the horizontal movement of the drone.
- \$\vec{v}_z\$ and \$\vec{a}_z\$ are the speed and acceleration vectors describing the vertical movement of the drone.
- *m* is the weight of payload.
- \vec{w}_{xy} is the vector of wind movement in the horizontal surface.
- $\beta_1, ..., \beta_9$ are the coefficients, and $\|\vec{v}\|$ denotes the magnitude of a vector.

The coefficients $\beta_1, ..., \beta_9$ can be estimated by the standard regression method, if sufficient measurement data is collected.

Assuming the uniform conditions (e.g., speed, wind) within a period of duration D, the total energy consumption of the drone in duration D is estimated by $\hat{P} \cdot D$.

3.3 Evaluation of Power Consumption Model

To evaluate the accuracy of the power consumption model, we conducted experiments to collect extensive empirical data to estimate the corresponding coefficients. Two test drones (3DR Solo and DJI Matrice 100) were used in two sets of experiments. A test drone was programmed to first fly vertical movements, then flying into a headwind and a tailwind with different weights of payloads. The drone maintained its altitude during the horizontal flight. We conducted experiments under simple conditions, where the drone ascended from the source until reaching the desired altitude and then flied directly to the destination without changing its altitude. But the experiments are sufficiently representative of other conditions.

The following are the estimated coefficients of power consumption models for 3DR Solo and DJI Matrice 100:

• 3DR Solo:

$$\hat{P}_{\text{solo}} = \begin{bmatrix} -1.526 \\ 3.934 \\ 0.968 \end{bmatrix}^{T} \begin{bmatrix} \|\vec{v}_{xy}\| \\ \|\vec{a}_{xy}\| \\ \|\vec{v}_{xy}\| \|\vec{a}_{xy}\| \end{bmatrix} + \begin{bmatrix} 18.125 \\ 96.613 \\ -1.085 \end{bmatrix}^{T} \begin{bmatrix} \|\vec{v}_{z}\| \\ \|\vec{a}_{z}\| \\ \|\vec{v}_{z}\| \|\vec{a}_{z}\| \end{bmatrix} + \begin{bmatrix} 0.220 \\ 1.332 \\ 433.9 \end{bmatrix}^{T} \begin{bmatrix} m \\ \vec{v}_{xy} \cdot \vec{w}_{xy} \end{bmatrix}$$
(2)

• DJI Matrice 100:

$$\hat{P}_{dji} = \begin{bmatrix} -2.595 \\ 0.116 \\ 0.824 \end{bmatrix}^T \begin{bmatrix} \|\vec{v}_{xy}\| \\ \|\vec{a}_{xy}\| \\ \|\vec{v}_{xy}\| \|\vec{a}_{xy}\| \end{bmatrix} + \begin{bmatrix} 18.321 \\ 31.745 \\ 13.282 \end{bmatrix}^T \begin{bmatrix} \|\vec{v}_z\| \\ \|\vec{a}_z\| \\ \|\vec{v}_z\| \|\vec{a}_z\| \end{bmatrix} + \begin{bmatrix} 0.197 \\ 1.43 \\ 251.7 \end{bmatrix}^T \begin{bmatrix} m \\ \vec{v}_{xy} \cdot \vec{w}_{xy} \end{bmatrix}$$
(3)

We discussed the evaluation results of the test two drones using ground truth power consumption data. Fig. 5-7 present the results for 3DR Solo, whereas Fig. 8-10 present the results for DJI Matrice 100. Fig. 5 and Fig. 8 depict the collected sensor data of our experiments for 3DR Solo and DJI Matrice 100, respectively. We tested 3 different weights of payloads under similar flight paths operations in each set of experiments. We obtain the estimated power consumption using the respective regression model, and compare it to the ground truth power consumption data shown in Fig. 6 and Fig. 9. We observe that the estimation is close to the actual measurement data. We integrate power over time to obtain the power consumption of the drone in Fig. 7 and Fig. 10. The errors of estimation of power consumption in the experiments are within 0.4%, showing relatively good accuracy of our power consumption models for both test drones.

4 FLIGHT MISSION PLANNING AND RECHARGING OPTIMIZATION

In this section, we utilize the calibrated power consumption model of a drone from the last section to study a joint problem of flight mission planning and recharging optimization for battery-operated autonomous drones. The objective is to complete a flight tour mission for a set of sites of interest in the shortest time. We consider a variable number of charging stations to allow recharging of drones intermediately. This problem naturally captures diverse applications of delivery and remote operations by drones. We provide efficient algorithms to determine the solutions, and implemented our algorithms in an automated drone management system.

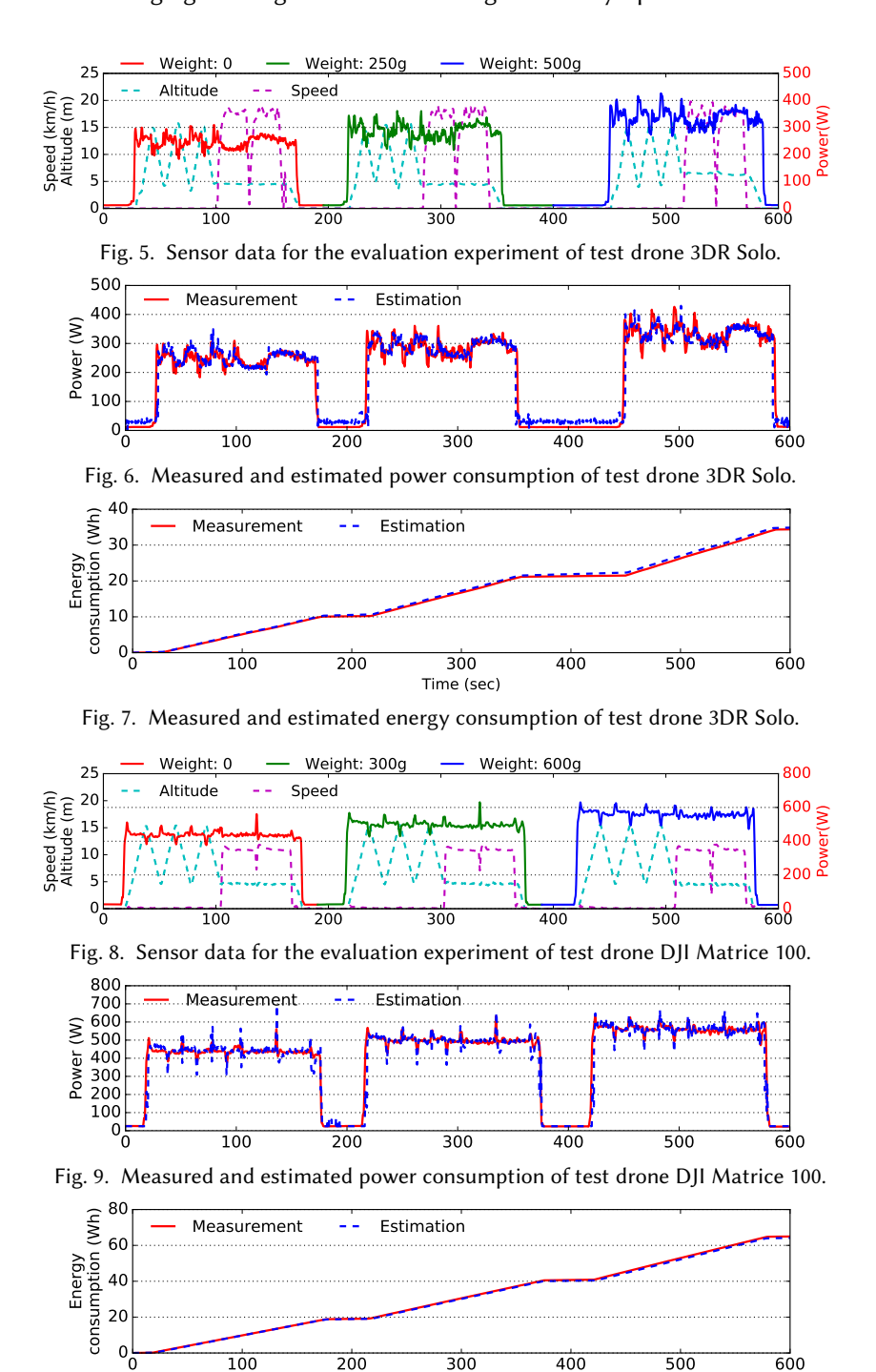


Fig. 10. Measured and estimated energy consumption of test drone DJI Matrice 100.

Time (sec)

4.1 Model and Formulation

We denote a set of sites of interest by S that a drone needs to visit (e.g., drop-off locations of parcels, or sites for measurements), and a set of charging station locations by C where a drone can receive recharging. The base location of a drone is denoted by v_0 . Let $V \triangleq S \cup C \cup \{v_0\}$. The problem of drone flight mission planning with recharging is to find a flight mission plan (which is a tour consisting of locations in S and C), such that the drone can visit all the sites in S, starting and terminating at v_0 , with an objective of minimizing the total trip time, while maintaining the state-of-charge (SoC) within the operational range. See an illustration of a flight mission plan with recharging for a drone in Fig. 11.



Fig. 11. A flight mission plan with recharging for a drone.

Given a pair of locations (u, v), we denote the designated flight path by $\ell(u, v)$, and the flight time by $\tau(u, v)$. In this paper, we consider a simple flight path, such that the drone first ascends vertically to a desired altitude, and then travels in a straight path, and finally descends to the destination vertically. The model can be generalized to consider non-straight paths.

Let $\mathsf{E}\big(\ell(u,v),\tau(u,v)\big)$ be the required energy consumption for the drone flying along $\ell(u,v)$ within flight time $\tau(u,v)$. $\mathsf{E}(\cdot,\cdot)$ is an increasing function that maps the combination of flight path $\ell(u,v)$ and flight time $\tau(u,v)$ to the required amount of energy. $\mathsf{E}(\cdot,\cdot)$ can be estimated by a power consumption model of a drone. We represent the charging strategy by a function $b(\cdot):C\mapsto\mathbb{R}$ that maps a charging station to an amount energy to be recharged. When recharging its battery at u, let the incurred charging time be $\tau_{\mathsf{c}}(b(u))$. Let $\eta_{\mathsf{c}} \leq 1$ and $\eta_{\mathsf{d}} \geq 1$ be the charging and discharging efficiency coefficients. If the drone flies to a charging station $u \in C$, it recharges its battery by an amount of energy denoted by $\eta_{\mathsf{c}}b(u)$. If the drone flies between two sites $u,v\in V$, then it consumes an amount of energy from the battery denoted by $\eta_{\mathsf{d}}\mathsf{E}\big(\ell(u,v),\tau(u,v)\big)$.

We denote a *flight mission plan* by \mathcal{F} , which is a tour starting and terminating at v_0 , consisting of a sequence of locations in $S \cup C \cup \{v_0\}$. Denote k-th location by \mathcal{F}_k . We require $\mathcal{F}_1 = \mathcal{F}_{|\mathcal{F}|} = v_0$. The objective of flight mission planning is to find a flight mission plan \mathcal{F} together with a charging strategy $b(\cdot)$ that minimizes the total trip time, consisting of the flight time plus the charging time.

Let x_k be the SoC when reaching the k-th location \mathcal{F}_k in the flight mission plan. We require the SoC to stay within feasible range $[\underline{B}, \overline{B}]$. The lower bound of SoC, \underline{B} , ensures sufficient residual energy for the drone to return to the base, in case of emergency. We set the initial SoC $x_0 = \overline{B}$.

With the above notations, the drone flight mission planning with recharging problem (DFP) is mathematically formulated as follows.

(DFP)
$$\min_{\mathcal{F},b(\cdot),x} \sum_{k=1}^{|\mathcal{F}|-1} \tau(\mathcal{F}_k,\mathcal{F}_{k+1}) + \sum_{k=1:\mathcal{F}_k \in C}^{|\mathcal{F}|} \tau_{c}(b(\mathcal{F}_k))$$
(4)

subject to

$$\mathcal{F}_1 = \mathcal{F}_{|\mathcal{F}|} = v_0 \tag{5}$$

$$S \subseteq \mathcal{F} \subseteq S \cup C \cup \{v_0\} \tag{6}$$

$$x_{k} = \begin{cases} x_{k-1} - \eta_{d} \mathsf{E} \Big(\ell(\mathcal{F}_{k}, \mathcal{F}_{k+1}), \tau(\mathcal{F}_{k}, \mathcal{F}_{k+1}) \Big), & \text{if } \mathcal{F}_{k} \in \mathcal{S} \\ x_{k-1} + \eta_{c} b(\mathcal{F}_{k+1}) - \eta_{d} \mathsf{E} \Big(\ell(\mathcal{F}_{k}, \mathcal{F}_{k+1}), \tau(\mathcal{F}_{k}, \mathcal{F}_{k+1}) \Big), & \text{if } \mathcal{F}_{k} \in \mathcal{C} \end{cases}$$
(7)

$$B \le x_k \le \overline{B}, \ x_0 = \overline{B} \tag{8}$$

The difficulty of DFP is to balance the flight decisions and charging decisions. On one hand, a flight mission plan needs to consider the requirement of completing the mission in minimal total trip time. On the other hand, it needs to be able to reach a charging station, in case of insufficient battery, as well as minimizing the charging time.

The formulation of DFP can be extended to incorporate a variety of further factors for practical flight mission plan optimization, such as restrictions of no-fly zones and attitude, and wind speed forecast information. Users can also specify further goals, such as deadline of completion and maximum payload weight. An efficient optimization algorithm is required to compute an optimal flight mission plan to meet the users' specified goals.

4.2 Case with Uniform Drone Speed and Steady Wind Condition

To provide efficient algorithms for DFP, we first consider a basic setting under some realistic assumptions. Suppose that the horizontal speed of the drone is a uniform constant under steady wind condition, which will be relaxed in Sec. 4.3. Then, the flight time $\tau(u,v)$ between two sites $u,v \in v$ is proportional to the length of flight path $\ell(u,v)$, denoted by d(u,v). Our regression model of energy consumption for drone in Sec. 3 implies that the function $\mathsf{E}\big(\ell(u,v),\tau(u,v)\big)$ is linear in the distance d(u,v), and the charging time $\tau_{\mathsf{c}}(b(u))$ is linear in the amount of recharged energy b(u). Thus, we assume the following linear objective functions:

$$\tau(u,v) = c_a d(u,v), \qquad \tau_c(b(u)) = c_b b(u), \tag{9}$$

$$\mathsf{E}\big(\ell(u,v),\tau(u,v)\big) = c_f(u,v) \cdot d(u,v),\tag{10}$$

for some constants $c_a, c_b, c_f(u, v) > 0$. Note that we allow $c_f(u, v)$ to be edge-dependent. This can model non-uniform environment for each $\ell(u, v)$, for instance, a path experiencing stronger wind is expected to have a larger constant $c_f(u, v)$.

Denote the lower and upper bounds of c_f by $\underline{c}_f \triangleq \min_{(u,v)} c_f(u,v)$ and $\overline{c}_f \triangleq \max_{(u,v)} c_f(u,v)$.

In this paper, we consider mostly long-distance trips (e.g., 2-3 km), for which the vertical landing and take-off operations usually constitute a small part of the whole flight, and consume only a small percentage of the total energy (e.g., < 1%). For clarity of presentation, we assume that the energy consumption of landing and take-off operations is implicitly captured by $c_f(u,v) \cdot d(u,v)$, though our results can be easily extended to consider that explicitly.

For convenience of notation, for a flight mission plan $(\mathcal{F}, b(\cdot))$, we write $\tau(\mathcal{F}) \triangleq \sum_{k=1}^{|\mathcal{F}|-1} \tau(\mathcal{F}_k, \mathcal{F}_{k+1})$ and $b(\mathcal{F}) \triangleq \sum_{k=1:\mathcal{F}_k \in \mathcal{C}}^{|\mathcal{F}|} \tau_c(b(\mathcal{F}_k))$. Also, define $d(\mathcal{F}) \triangleq \sum_{k=1}^{|\mathcal{F}|-1} d(\mathcal{F}_k, \mathcal{F}_{k+1})$.

Under the aforementioned assumptions, the total charging time $\tau_c(b(\mathcal{F}))$, in an optimal flight mission plan \mathcal{F} , is proportional to the total flight time $\tau(\mathcal{F})$, by the following lemma.

LEMMA 4.1. In an optimal flight mission plan $(\mathcal{F}, b(\cdot))$, we have

$$c \cdot d(\mathcal{F}) + c' \le \tau(\mathcal{F}) + \tau_c(b(\mathcal{F})) \le \overline{c} \cdot d(\mathcal{F}) + c'$$

where either

1)
$$\underline{c} = \overline{c} = c_a$$
 and $c' = 0$, or
2) $\underline{c} = c_a + \underline{c}_f c_b \frac{\eta_d}{\eta_c}$, $\overline{c} = c_a + \overline{c}_f c_b \frac{\eta_d}{\eta_c}$, and $c' = \frac{c_b}{\eta_c} (\underline{B} - x_0)$.

Proof. See the Appendix.

Lemma 4.2. Given any feasible flight mission plan $(\mathcal{F}, b(\cdot))$, there is another feasible flight mission plan $(\mathcal{F}, b'(\cdot))$ such that

$$\tau_{\rm c}(b(\mathcal{F})) \leq \frac{\underline{B} - x_0}{\eta_{\rm c}} + \frac{\overline{c}_f \eta_{\rm d}}{\eta_{\rm c}} \cdot d(\mathcal{F})$$

Such a plan $(\mathcal{F}, b'(\cdot))$ can be found in O(|V|) time.

Proof. See the Appendix.

Both Lemma 4.1 and Lemma 4.2 allow us to focus on minimizing the distance $d(\mathcal{F})$ instead of total trip time. Hence, we simplify the problem DFP as a simplified formulation (SDFP), such that its optimal solution is later shown to be within a constant factor with an optimal solution of DFP. Simplified formulation (SDFP) is defined as follows.

(SDFP)
$$\min_{\mathcal{F},x} \sum_{k=1}^{|\mathcal{F}|-1} \widehat{d}(\mathcal{F}_k, \mathcal{F}_{k+1})$$
 (11)

subject to
$$\mathcal{F}_1 = \mathcal{F}_{|\mathcal{F}|} = v_0$$
 (12)

$$S \subseteq \mathcal{F} \subseteq S \cup C \cup \{v_0\} \tag{13}$$

$$x_{k} = \begin{cases} x_{k-1} - \eta_{d} \widehat{d}(\mathcal{F}_{k}, \mathcal{F}_{k+1}), & \text{if } \mathcal{F}_{k} \in \mathcal{S} \\ \overline{B}, & \text{if } \mathcal{F}_{k} \in \mathcal{C} \end{cases}$$
(14)

$$\underline{B} \le x_k \le \overline{B}, \ x_0 = \overline{B} \tag{15}$$

In SDFP, we consider a modified distance function $\widehat{d}(\cdot,\cdot)$, which is defined as follows. Recall that $V \triangleq S \cup C \cup \{v_0\}$. Consider a weighted undirected graph $G_0 = (V, \binom{V}{2})$, whose edge lengths are defined by $\{c_f(u,v)\cdot d(u,v)\}_{u,v}$. Then, obtain $\{\widehat{d}(u,v)\}_{u,v}$, which are the pairwise shortest distances of each pair of nodes in G₀. SDFP is related to the tour gas station problem in [15], which optimizes a tour trip of a vehicle in minimal fuel cost, with options of refilling at given gas stations.

Note that we assume in the formulation of SDFP that the SoC is brought to its maximum at each charging station. Once we obtain a tour under this assumption, it can be turned into a flight mission plan with the minimal charging requirements using Lemma 4.2.

For $u \in V$, let $\widehat{d}_u \triangleq \min_{v \in C} \widehat{d}(u, v)$ be the distance to the nearest charging station from v, and $s_u \triangleq \operatorname{argmin}_{v \in C} \widehat{d}(u, v)$ be the nearest charging station from v.

Define $U \triangleq \frac{B-B}{\eta_d}$. Following [15], we make a mild assumption that for every $u \in S \setminus \{v_0\}$ there is $v \in C$ such that $d(u,v) \le \alpha \frac{U}{2}$, where $\alpha \in [0,1)$. This assumption can be justified (for $\alpha = 1$) as follows. For a location $u \in S \setminus \{v_0\}$, if every $v \in C$ is at distance greater than $\frac{U}{2}$, then it is infeasible to visit u without incurring the battery level below \underline{B} (as the SoC drops below $\overline{B} - \eta_d U = \underline{B}$).

In the following, we present an algorithm to SDFP and then DFP. The main algorithm is Find-plan[V,d], which is a variant of Christofides Algorithm [7] for finding a tour for travelling salesman problem, based on the results in [15]. It finds a minimum spanning tree T, and then a minimum weight perfect matching M on the odd vertices of T. The edges of T and M define an Eulerian graph, from which an Eulerian tour \mathcal{F}_0 can be obtained in linear time. The Eulerian tour is passed to the procedure Fix-plan for converting it to a feasible flight mission plan \mathcal{F} , which might use a non-optimal charging function $b(\cdot)$. Then, the resulting plan $(\mathcal{F},b(\cdot))$ is further passed to procedure Fix-charge for finding the minimal charging requirements with respect to the flight mission plan \mathcal{F} . Specifically, the three procedures in Find-plan [V,d] are:

- Init-distances $[V, \widehat{d}, u, v]$: This provides a lower bound for an optimal solution. Namely, it finds for every pair of locations $u, v \in V$, the minimum possible distance $\widetilde{d}(u, v)$, and the corresponding shortest path $\mathcal{P}(u, v)$ to go from u to v without going out of the operational range of the battery. Note that if $\widehat{d}(u, v) \leq U \widehat{d}_u \widehat{d}_v$ then the drone can always go directly from u to v^1 . Otherwise, at best (in an optimal solution), the drone can reach u with SoC at most $\overline{B} \eta_{\mathrm{d}}\widehat{d}_u$, then it can visits a sequence of charging stations (only if the distance \widehat{d} between two successive such stations is at most U), then, form the last station, it has to reach v such that the SoC at v is at least $\underline{B} + \eta_{\mathrm{d}}\widehat{d}_v$ (so that there is sufficient battery to reach v). In particular, the distance from v to the first charging station on this path should be at most v0 and v1. This explains the definition of the graph v3 in line 5 of the procedure.
- Fix-plan $[G, \mathcal{F}_0]$: starting from the flight mission plan \mathcal{F}_0 obtained using the (modified) Christofides algorithm with respect to the weights \widetilde{d} , this procedure reconstructs a feasible flight mission plan \mathcal{F} for problem (SDFP). It first replaces each edge (u, v) in the flight mission plan by the corresponding path $\mathcal{P}(u, v)$. Since the resulting flight mission plan maybe still infeasible, the procedure adds to every site a round trip to the closest charging station. Finally, the added stations are dropped one by one in a greedy way as long as feasibility is maintained.
- Fix-charge $[\mathcal{F}, b(\cdot)]$: Starting from the flight mission plan $(\mathcal{F}, b(\cdot))$ constructed after calling procedure Fix-plan $[G, \mathcal{F}_0]$, this procedure finds a minimal amount of recharging energy, according to Lemma 4.2.

Let OPT_{DFP} and OPT_{SDFP} be the optimal solutions of problems (DFP) and (SDFP), respectively.

LEMMA 4.3 ([15]). The flight mission plan \mathcal{F} returned by algorithm Find-plan [V,d] has cost $\widehat{d}(\mathcal{F}) \leq \frac{3}{2} \left(\frac{1+\alpha}{1-\alpha}\right) \mathsf{OPT}_{\mathsf{SDFP}}.$

The following theorem establishes that algorithm Find-plan [V, d] has an asymptotic constant-factor approximation guarantee for DFP.

THEOREM 4.4. The flight mission plan $(\mathcal{F}, b'(\cdot))$ returned by algorithm Find-plan [V, d] has cost $\tau(\mathcal{F}) + \tau_c(b(\mathcal{F})) = O(\mathsf{OPT}_\mathsf{DFP}) + O(1)$.

Proof. See the Appendix.

¹That is, starting with SoC = \overline{B} at \mathbf{s}_u , then the drone reaches u with SoC $\overline{B} - \eta_{\mathrm{d}}\widehat{d}_u$, and then it flies directly from u to v causing the SoC to drop to $\overline{B} - \eta_{\mathrm{d}}(\widehat{d}_u + \widehat{d}(u, v)) = \underline{B} + \eta_{\mathrm{d}}(U - \widehat{d}_u - \widehat{d}(u, v)) \geq \underline{B} + \eta_{\mathrm{d}}\widehat{d}_v$ at v. Thus, there is sufficient battery at v to reach \mathbf{s}_v .

Algorithm 1 Find-plan [V, d]

```
1: Compute pairwise shortest distances \{\widehat{d}(u,v)\}_{u,v} on weighted undirected graph G_0 = (V, \binom{V}{2})

2: for each u,v \in V do

3: (\widetilde{d}(u,v),\mathcal{P}(u,v)) \leftarrow \text{Init-distances}[V,\widehat{d},u,v]

4: end for

5: Consider the weighted undirected graph G = (V,E;\widetilde{d}) where E = \binom{V}{2}

6: Find a minimum spanning tree T = (V,E_T) in G

7: V_0 \leftarrow \text{find} the set of odd degree vertices in T

8: Find a minimum-weight perfect matching M = (V_0,E_M) in the graph (V_0,E;\widetilde{d})

9: \mathcal{F}_0 \leftarrow \text{find} an Eulerian tour in the graph (V,E_T \cup E_M)

10: \mathcal{F} \leftarrow \text{Fix-plan}[G,\mathcal{F}_0]

11: b'(\cdot) \leftarrow \text{Fix-charge}[\mathcal{F},b(\cdot)]

12: return (\mathcal{F},b'(\cdot))
```

Algorithm 2 Init-distances $\left[V,\widehat{d},u,v\right]$

```
1: if \widehat{d}(u,v) \leq U - \widehat{d}_u - \widehat{d}_v then
2: \widehat{d}(u,v) \leftarrow \widehat{d}(u,v), \mathcal{P}(u,v) \leftarrow \{(u,v)\}
3: return (\widehat{d}(u,v),\mathcal{P}(u,v))
4: else
5: Construct a weighted undirected graph G = (C \cup \{u,v\}, E; w) where E \triangleq \left\{\{u,z\}: z \in C, \widehat{d}(u,z) \leq U - \widehat{d}_u\right\} \cup \left\{\{v,z\}: z \in C, \widehat{d}(v,z) \leq U - d'_v\right\} \cup \left\{\{z,z'\}: z,z' \in C, \widehat{d}(z,z') \leq U\right\} and w(z,z') \triangleq \widehat{d}(z,z') for all z,z' \in C \cup \{u,v\}
6: \mathcal{P}(u,v) \leftarrow shortest path between u and v in G (with a set of edge lengths \{w(u,v)\}_{u,v})
7: \widehat{d}(u,v) \leftarrow length of \mathcal{P}(u,v)
8: return (\widehat{d}(u,v),\mathcal{P}(u,v))
9: end if
```

Algorithm 3 Fix-plan $[G, \mathcal{F}_0]$

```
1: \mathcal{F} \leftarrow \emptyset

2: for each (u, v) in \mathcal{F}_0 do

3: Add \mathcal{P}(u, v) to \mathcal{F}

4: end for

5: Add to \mathcal{F} a set of sub-tours \{\{(u, s_u), (s_u, u) : u \in V\}

6: for u \in V do

7: if \mathcal{F} \setminus \{(u, s_u), (s_u, u) \text{ is feasible then}

8: \mathcal{F} \leftarrow \mathcal{F} \setminus \{(u, s_u), (s_u, u)\}

9: end if

10: end for

11: return \mathcal{F}
```

Algorithm 4 Fix-charge $[\mathcal{F}, b(\cdot)]$

```
1: Let \mathcal{F}_{i_1}, \dots, \mathcal{F}_{i_r} be the charging stations, in the order they appear on \mathcal{F}
2: \mathbf{for}\ j = 0, 1, \dots, r\ \mathbf{do}
3: D_j = \eta_{\mathbf{d}} \sum_{k=i_j}^{i_{j+1}-1} c_f(\mathcal{F}_k, \mathcal{F}_{k+1}) d(\mathcal{F}_k, \mathcal{F}_{k+1})
4: \mathbf{end}\ \mathbf{for}
5: \mathbf{for}\ j = 1, \dots, r\ \mathbf{do}
6: B_j \triangleq \eta_{\mathbf{c}} \sum_{k=1}^{j} b(\mathcal{F}_{i_k})
7: \mathbf{end}\ \mathbf{for}
8: \mathbf{for}\ j = r\ \mathbf{downto}\ 1\ \mathbf{do}
9: b'(\mathcal{F}_{i_j}) = \max\{0, \frac{1}{\eta_{\mathbf{c}}}(\underline{B} - x_0 + \sum_{k=0}^{r} D_k - \sum_{k=1}^{j-1} B_k)\}
10: \mathbf{if}\ b'(\mathcal{F}_{i_j}) > 0\ \mathbf{then}
11: \mathbf{exit}
12: \mathbf{end}\ \mathbf{if}
13: \mathbf{end}\ \mathbf{for}
14: \mathbf{return}\ b'(\cdot)
```

4.3 Extensions

The preceding section presents a basic setting of DFP and its efficient algorithms. In reality, an automated drone management system requires more sophisticated options. In this section, we present two extensions to the preceding algorithms to obtain heuristics for more practical scenarios.

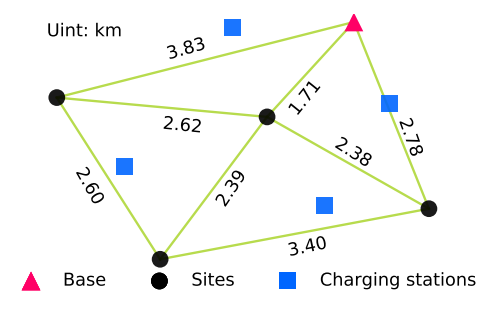
- 4.3.1 Wind Uncertainty. Under steady wind condition, we assume in the preceding algorithms that $c_f(u,v)$ is a constant that depends on the designated path between sites u and v. In practice, there is sometimes uncertainty in the wind condition. Often, the wind varies as the drone flies. This also depends on the expected wind condition on this path. Thus, it should be more precisely represented by $c_f(u,v,w)$, where w is the wind vector whose value is in an uncertain domain $w \in W$. For example, W is defined by the predicted speed range $[\underline{|w|}, \overline{|w|}]$ and the predicted orientation range $[\underline{\theta}_w, \overline{\theta}_w]$. We can modify the algorithms to account for the uncertainty of W. We proceed conservatively in our algorithm by taking the worst-case, replacing $c_f(u,v)$ by $\overline{c}_f(u,v) = \max_{w \in W} c_f(u,v,w)$.
- 4.3.2 Variable Drone Speed. We consider another scenario, in which the drone can vary its speed uniformly at all designated paths in V. In this case, we run our algorithms sequentially in multiple rounds, with an increasing drone speed at each round, until the algorithms can not return a feasible solution (because that higher drone speed may result in insufficient battery to reach some sites). Then we will enumerate all the optimal solutions in all the rounds to find the best solution with the lowest total flight time. By enumerating the possibilities of different drone speeds, the algorithms can identify an optimal flight mission plan.

5 CASE STUDIES

We implemented the algorithms in an automated drone management system. In particular, we evaluated the results of flight mission planning and recharging optimization for the test drones in several case studies, based on the data from empirical studies.

5.1 Setup

We consider a scenario with four sites of interest, and four charging stations. The drones are programmed to begin its mission from the base. Fig. 12 depicts the geographical locations of the sites (as black points), charging stations (as blue squares) and the base (as magenta triangle). The choices of geographical locations and distances are based on some real locations of a suburban community.



Case	Drone	Battery (Wh)	$\ \vec{w}_{xy}\ $ (20 km/h)	m (g)
1	Solo	70	South	0
2	Solo	70	North-East	0
3	Solo	140	South	500
4	Solo	140	North-East	500
5	DJI	130	South	0
6	DJI	130	North-East	0
7	DJI	260	South	600
8	DJI	260	North-East	600

Fig. 12. Geographical locations of the sites, charging stations and base.

Fig. 13. Parameters of setup.

There are two major sets of studies conducted as follows.

- (1) Study 1: We study eight sub-cases using the power consumption models of 3DR Solo and DJI Matrice 100 under different wind and payload conditions. For each drone, we study 4 sub-cases as follows. We consider using one battery in the first two sub-cases of each drone. Different wind conditions with average wind speed of 18 km/h are studied in the sub-cases. Then we double the battery capacity with the same wind condition in another two sub-cases. Since the battery capacity is doubled, extra weight is added to the drone. The parameters of all the sub-cases are summarized in Table 13.
- (2) *Study 2*: We consider uncertainty of wind conditions. The wind speed and orientation vary within a certain range. The wind speed varies from 0 to 21 km/h in four discrete scales, while the wind orientation varies from 0° to 360° in four discrete scales.

In Study 1, the cases of 3DR Solo are denoted by S_1C_1 to S_1C_4 , and the cases of DJI Matrice 100 are denoted by S_1C_5 to S_1C_8 . Similarly, in Study 2, the cases of 3DR Solo are denoted by S_2C_1 to S_2C_4 , and the cases of DJI Matrice 100 are denoted by S_2C_5 to S_2C_8 .

5.2 Results and Discussion

For comparison, we also consider a *benchmark* algorithm, by which a drone flies to the nearest unvisited site, or the SoC drops below a preset threshold, then the drone flies to a charging station instead. We set the preset threshold to be the minimum SoC that can fly to a nearest charging station from any site.

- 5.2.1 Study 1. The results of flight missions of Study 1 are visualized in Figs. 16-19. The numbers indicate the path order of the drone. The colors represent the SoC of battery. The wind orientations are displayed on the upper-left corners. We plot the trip time and energy consumption of Study 1 in Figs. 14-15. There are several interesting observations as follows:
 - Our algorithm significantly outperforms the benchmark algorithm, in terms of trip time and energy consumption. Hence, our algorithms are superior for flight mission planning.

- In the case study, the north-east wind affects flight missions to a larger extent, which causes a higher energy consumption than that by south wind. Besides, there is a longer trip time due to longer charging time.
- We observe that even the trip times in S₁C₇ and S₁C₈ are shorter, it consumes more energy since the drone carrying extra battery, which results in heavier loads.
- Attaching one more battery does not help to reduce the trip time for 3DR Solo, while attaching more battery helps to reduce trip time for DJI Matrice 100. The reason is because attaching more battery enables DJI Matrice 100 to fly longer without recharging. The total trip time is significantly decreased due to much shorter charging time (as the blue bars of S₁C₇ and S₁C₈ are shorter). But the same path is not feasible for 3DR Solo. 3DR Solo will require to charge at the left most charging station, and hence, the trip time increases. If we slightly increase the battery capacity to 75 Wh, the results of 3DR Solo will be the same as that of DJI Matrice 100.

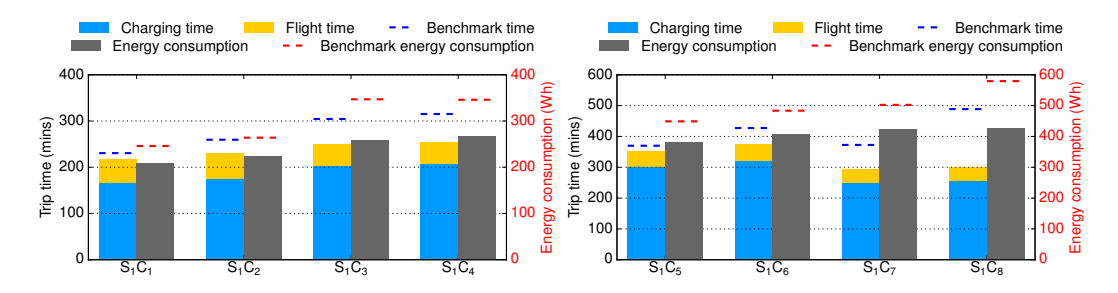


Fig. 14. Trip time and energy consumption of Study 1 Fig. 15. Trip time and energy consumption of Study 1 using 3DR Solo.

Graph 14. Trip time and energy consumption of Study 1 using DJI Matrice 100.

5.2.2 Study 2. We study the results of flight mission planning considering uncertainty of wind condition. We consider two sub-cases with the shortest trip time of two different drones from Study 1 (i.e., S_1C_1 and S_1C_7) and then increase uncertainty level for each case.

The results of flight missions of Study 2 are visualized in Figs. 20-21. We represent the ranges of wind speeds and orientations as the shaded areas on the upper-left circles. We plot the trip time and energy consumption of Study 2 in Figs. 22-23. There are several observations as follows:

- Recall that the energy consumption of S₁C₁ does not have uncertain wind condition for 3DR Solo with 70 Wh battery. In Study 2, we investigate if a feasible solution can be obtained in the presence of uncertainty of wind condition. We gradually increase the uncertainty from S₂C₁ to S₂C₄. For example, in S₂C₁ the wind speed varies from 9 to 12 km/h and orientation varies from -45° to 45°. In this case, our algorithms always consider the worst-case setting in the given range of wind conditions.
- We observe that the energy consumption in general increases as the uncertainty of wind condition increases in Fig. 22. In partcular, the energy consumption of the worst uncertainty is in S_2C_4 , in which the drone may always fly into a tailwind. Thus, S_2C_4 provides the most conservative result.
- \bullet Similarly, recall that the energy consumption of S_1C_7 does not have uncertain wind condition for DJI Matrice 100 with 260 Wh battery (two batteries). We also observe similar trends when the wind uncertainty is increased. In general, when uncertainty increases, the difference of trip time/energy consumption between our approach and benchmark becomes smaller. This is because of more frequent recharging when the uncertainty becomes larger.

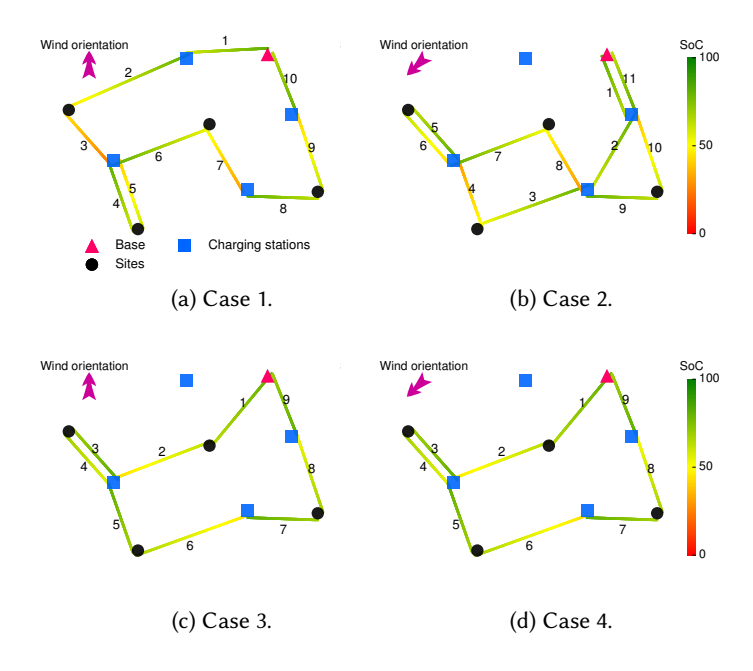


Fig. 16. Visualized flight missions for Study 1 using 3DR Solo by our algorithm.

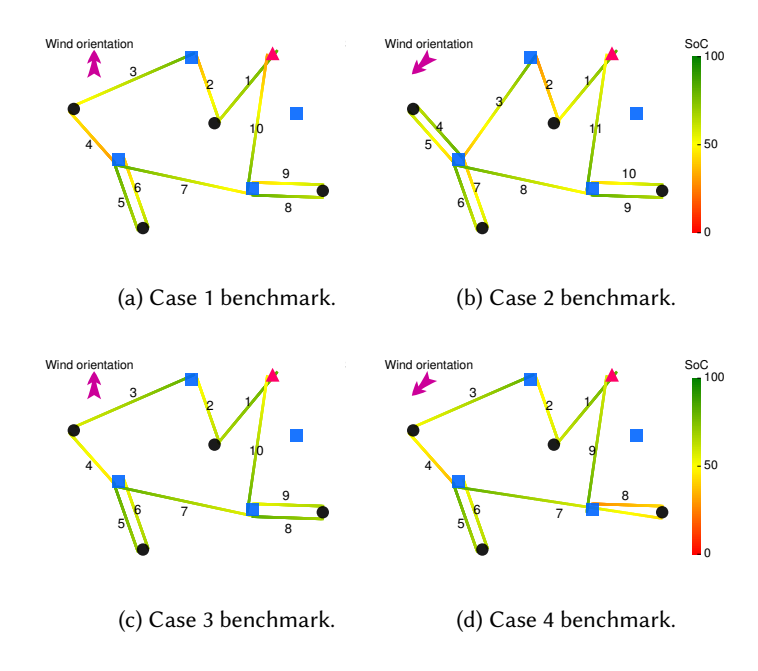


Fig. 17. Visualized flight missions for Study 1 using 3DR Solo by benchmark algorithm.

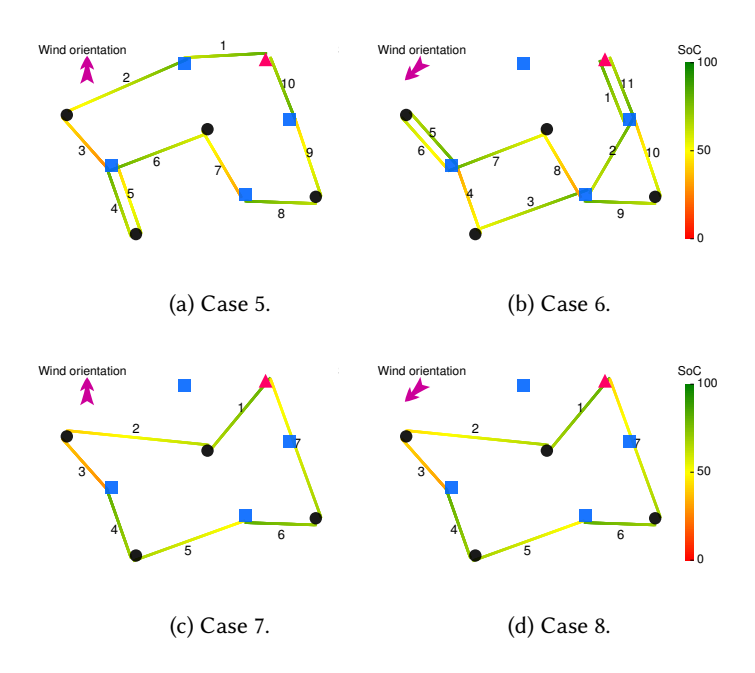


Fig. 18. Visualized flight missions for Study 1 using DJI Matrice 100 by our algorithm.

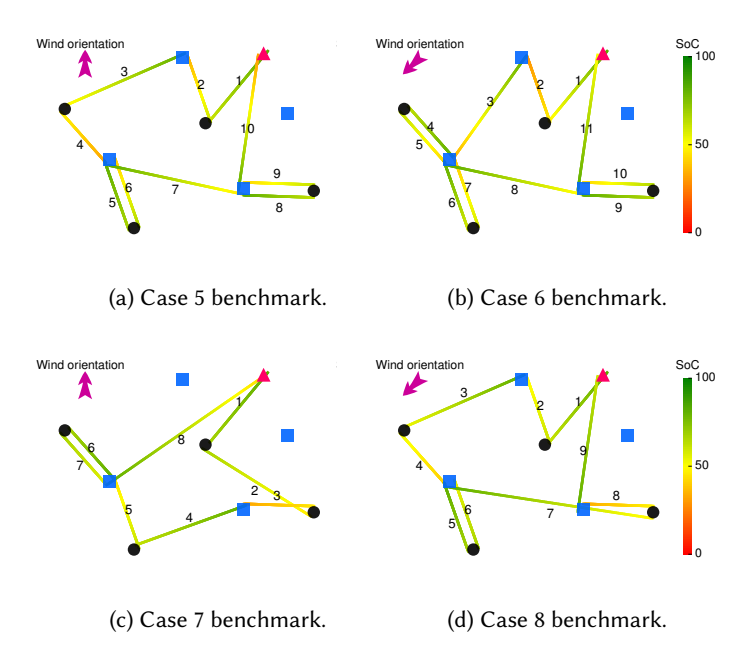


Fig. 19. Visualized flight missions for Study 1 using Matrice 100 by benchmark algorithm.

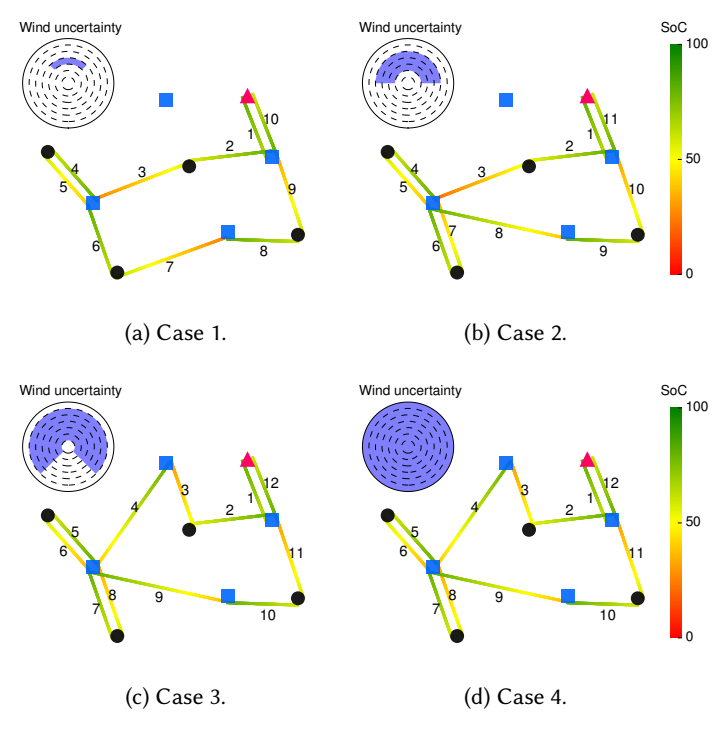


Fig. 20. Visualized flight missions for Study 2 using 3DR Solo.

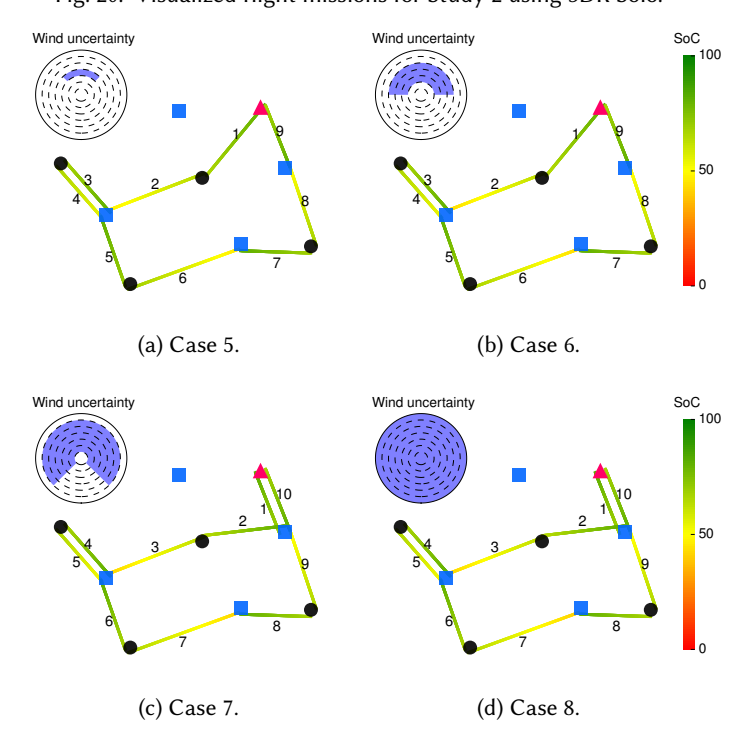


Fig. 21. Visualized flight missions for Study 2 using DJI Matrice 100.

, Vol. 1, No. 1, Article 1. Publication date: January 2017.

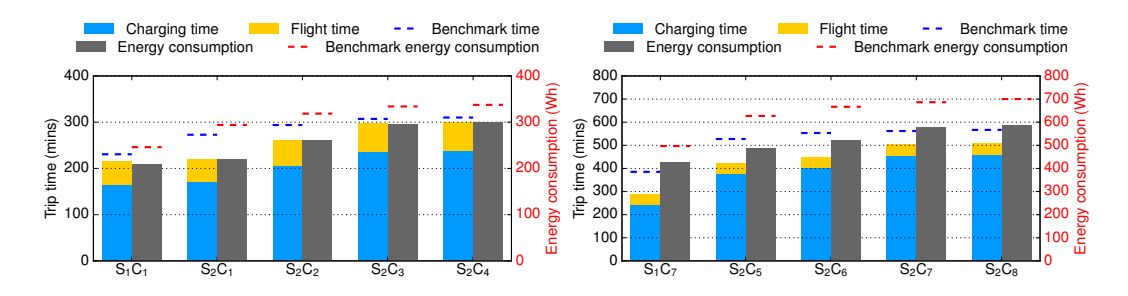


Fig. 22. Trip time and energy consumption of Study Fig. 23. Trip time and energy consumption of Study 2 using 3DR Solo. 2 using DJI Matrice 100.

6 AUTOMATED DRONE MANAGEMENT SYSTEM

We implemented our algorithms in an automated drone management system. The user interface is depicted in Fig 24. The user interface allows the users to specify individual goals and to visualize the computed flight mission plan. The system connects to a cloud computing server, which uses the input locations from the user and computes the optimal flight mission plan. Then the drone is programmed to follow the flight mission plan computed by the server.

Furthermore, a dynamic tracking system of drone using on-board sensors, including GPS location, video feed, SoC, and flight status, is utilized to monitor the real-time flight status of the drone. If abnormal measurements are detected, for example, the reported sensor measurements deviate from estimated value by flight mission planning, then real-time re-computation will be performed to find the minimum adjustment to the previously computed flight mission plan. The user can abort the mission anytime by clicking the button on the system. We remark that multiple drones can also be tracked simultaneously.

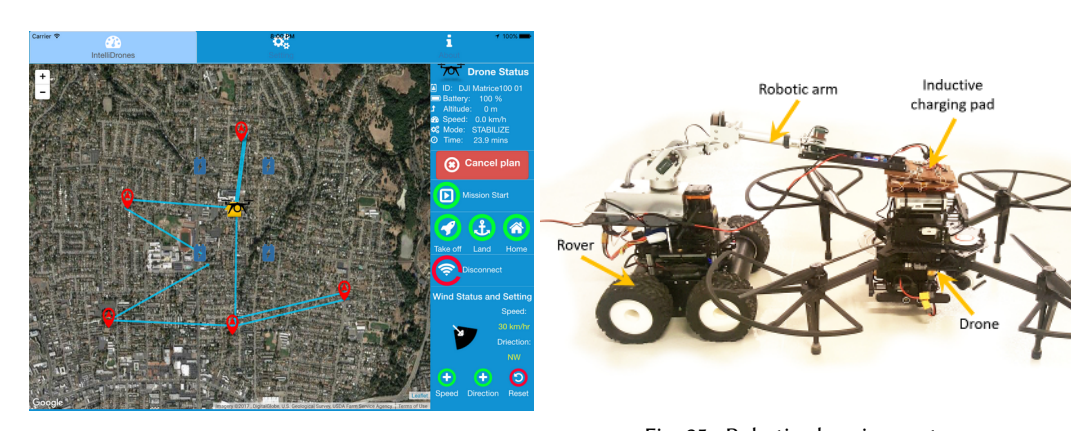


Fig. 24. Interface of automated drone management system.

Fig. 25. Robotic charging system.

7 AUTONOMOUS ROBOTIC CHARGING SYSTEM PROTOTYPE

In this section, we present a robotic charging system prototype that can recharge drones autonomously by our drone management system. More technical details can be found in [14].

There is a tethered rover capable of autonomous navigation, equipped with a robotic arm carrying a charging pad that can adapt to different drone sizes and landing positions (see Fig. 25). Our robotic rover uses 2D Light Detection and Ranging (LIDAR) sensors to navigate and detect a drone. LIDAR sensors are more robust to environmental uncertainties and external lighting conditions than computer vision sensors. The robotic charging system is comprised of three main components:

- **Charging system**: Since the goal of the charging system is to recharge drones in remote areas, disconnected from the grid, it is vital to provide self-generating charging system, as well as to protect the robotic rover from harsh environment conditions (i.e., rain, the wind, etc.) when idle. So, our prototype can be powered by a solar panel. A landing zone with an area of at least 3×3 m² is designated for drone landing in front of the charging system.
- **Robotic rover**: To enable flexible deployment, a tethered rover is equipped with a robotic arm that mounts a wireless inductive transmitter. Using autonomous drone detection and navigation, the rover can cater for arbitrary landing position and orientation of a drone, which is the case for most commercial drones that solely rely on inaccurate GPS and Inertial Measurement Unit (IMU) for landing.
- **Drones**: Each drone is equipped with an inductive wireless receiver, compatible with that of the robotic rover. In order to recharge a drone, the drone management system will send a signal to the charging system to initiate the charging procedure.

We use Hokuyo UTM-30LX Scanning Laser Rangefinder to obtain 2D point cloud. The laser rangefinder provides 30 meters detection range which allows the rover to detect far objects such as drones or obstacles. The detection angle is 270° with 0.25° angular resolution. The rover odometry is obtained based on wheel rotation using quadrature encoders.

A retractable arm is used to conduct inductive charging for the drones, which can flexibly recharge drones in arbitrary positions. The inductive charging technology is based on resonant inductive coupling, which can transfer energy without physical contact. It has been widely used in wireless charging for smart phones. The use of inductive charging technology facilitates a fully automated drone management system, without manually plugging to an external charger. The current prototype uses six coils for inductive charging, giving a maximum charging speed of $6 \times 700 = 3500$ mA. We mounted six current sensors, on the robotic arm, to measure individual coil charging rate. Our test drone is DJI Matrice 100 which is powered by two 5700 mA on-board Li-Poly battery.

7.1 Recharging Process

We next describe the operations of recharging process. Once a drone is landed and a recharging command is initiated, the robotic rover proceeds as follows:

- (1) *Finding the drone:* From raw 2D LIDAR point cloud, we use a clustering technique to separate the points of the drone from the background points.
- (2) Classifying the drone and detecting its orientation: Based on supervised learning, drone information (e.g., type, size, orientation, etc.) can be extracted from point cloud data. We consider a single drone, and its orientation is detected using a rectangle boundary model. The orientation of the drone is needed to instruct the rover to navigate to a position that supports a better alignment for the charging pad with the receiver on the drone. This allows more flexibility in the charging pad design (e.g., rectangular inductive charging pad instead of a circular pad) to fit more inductive coils on the drone.
- (3) *Autonomously navigating towards the drone*: the exact position of the navigation goal is determined based on the allowable charging position.

(4) Recharging: Position the charging pad on the drone and adjust the positioning using current sensors readings.

Once a drone is fully charged, a termination command is initiated to the charging system. Then the rover returns to the charging system to resume its idle state. Also, the drone management system actively communicates with the robotic charging system to track the charging status.

CONCLUSION

Automated drone management system is important for practical applications of drones. This paper provides multiple contributions to automated management systems for battery-operated drones, including empirical studies to model the battery performance of drones considering various flight scenarios, a study of flight mission planning and recharging optimization for drones that captures diverse applications of delivery and remote operations by drones, and a management system implementation with a robotic charging station to support autonomous recharging of drones.

In future work, we will incorporate a variety of further features in our automated drone management system, such as restrictions of no-fly zones and attitude, and wind speed forecast. Users may also be able to specify further goals, such as deadline of completion and maximum payload weight.

PROOFS Α

Lemma 4.1. In an optimal flight mission plan $(\mathcal{F}, b(\cdot))$, we have

$$c \cdot d(\mathcal{F}) + c' \le \tau(\mathcal{F}) + \tau_c(b(\mathcal{F})) \le \overline{c} \cdot d(\mathcal{F}) + c'$$

where either

1)
$$\underline{c} = \overline{c} = c_a$$
 and $c' = 0$, or
2) $\underline{c} = c_a + \underline{c}_f c_b \frac{\eta_d}{\eta_c}$, $\overline{c} = c_a + \overline{c}_f c_b \frac{\eta_d}{\eta_c}$, and $c' = \frac{c_b}{\eta_c} (\underline{B} - x_0)$.

Proof. Consider an optimal flight plan $(\mathcal{F},b(\cdot))$ and assume that the charging stations, in the order they appear on \mathcal{F} , is $\mathcal{F}_{i_1}, \dots, \mathcal{F}_{i_r}$, where without loss of generality, we assume $\mathcal{F}_{i_1} \neq v_0$.

For completeness, let $i_0 \triangleq 1$ and $i_{r+1} \triangleq |\mathcal{F}|$. For $j = 0, 1, \dots, r$, let

$$D_{j} \triangleq \eta_{\mathrm{d}} \sum_{k=i_{j}}^{i_{j+1}-1} c_{f}(\mathcal{F}_{k}, \mathcal{F}_{k+1}) \cdot d(\mathcal{F}_{k}, \mathcal{F}_{k+1}),$$

and for j = 1, ..., r, let $B_j \triangleq \eta_c b(\mathcal{F}_{i_j})$.

Then, the feasibility of the flight mission plan ${\mathcal F}$ implies

$$x_0 - \sum_{k=0}^{j} D_k + \sum_{k=1}^{j} B_k \ge \underline{B}, \text{ for } j = 0, \dots, r$$

$$\tag{16}$$

Let us refer to Ineq. (16) for a particular j as $I(j) \ge \underline{B}$. Particularly, consider $I(r) \ge \underline{B}$. Suppose that this inequality is not tight, that is, the left-hand side is strictly larger than the right-hand side. Note that the variable $b(\mathcal{F}_{i_r}) = \frac{B_r}{\eta_c}$ appears only in this inequality. Since $b(\mathcal{F}_{i_r})$ appears in the objective function $\tau_c(b(\mathcal{F}))$ with a positive coefficient (i.e., $\tau_c(b(u)) = c_b b(u)$), there are two cases: (i) $b(\mathcal{F}_{i_r}) = 0$ at optimality, if $I(r) > \underline{B}$, or (ii) $b(\mathcal{F}_{i_r}) > 0$ at optimality, if $I(r) = \underline{B}$. Otherwise, it will contradict to the optimality of $b(\mathcal{F}_{i_r})$, by reducing the value of $b(\mathcal{F}_{i_r})$. If it is case (i), then the inequality $I(r-1) \ge \underline{B}$ becomes redundant (as $I(r-1) \ge I(r) > 0$). Removing $I(r-1) \ge \underline{B}$, we obtain that the variable $b(\mathcal{F}_{i_{r-1}})$ appears only in $I(r) \geq \underline{B}$. Similarly, we can conclude that $b(\mathcal{F}_{i_{r-1}}) = 0$ and remove the (now) redundant inequality $I(r-2) \ge \underline{B}$.

Continuing this argument, we conclude that there are two cases: (1) either all variables $b(\mathcal{F}_{i_j})$ are set to zero in which case the value of the objective is $\tau(\mathcal{F}) = c_a d(\mathcal{F})$, or (2) we have

$$x_0 - \sum_{k=0}^r D_k + \sum_{k=1}^r B_k = \underline{B},$$

In case (2), the value of the objective is

$$\tau(\mathcal{F}) + \frac{c_b}{\eta_c} \sum_{k=1}^r B_k = \tau(\mathcal{F}) + \frac{c_b}{\eta_c} (\underline{B} - x_0 + \sum_{k=0}^r D_k)$$
$$= \tau(\mathcal{F}) + \frac{c_b}{\eta_c} \sum_{k=0}^r D_k + \frac{c_b}{\eta_c} (\underline{B} - x_0)$$

Therefore,

$$\begin{split} \left(c_a + \underline{c}_f c_b \frac{\eta_{\rm d}}{\eta_{\rm c}}\right) d(\mathcal{F}) + \frac{c_b}{\eta_{\rm c}} (\underline{B} - x_0) \leq \tau(\mathcal{F}) + \frac{c_b}{\eta_{\rm c}} \sum_{k=0}^r D_k + \frac{c_b}{\eta_{\rm c}} (\underline{B} - x_0) \\ \leq \left(c_a + \overline{c}_f c_b \frac{\eta_{\rm d}}{\eta_{\rm c}}\right) d(\mathcal{F}) + \frac{c_b}{\eta_{\rm c}} (\underline{B} - x_0). \end{split}$$

Lemma 4.2. Given any feasible flight mission plan $(\mathcal{F}, b(\cdot))$, there is another feasible flight mission plan $(\mathcal{F}, b'(\cdot))$ such that

$$\tau_{\rm c}(b(\mathcal{F})) \leq \frac{\underline{B} - x_0}{\eta_{\rm c}} + \frac{\overline{c}_f \eta_{\rm d}}{\eta_{\rm c}} \cdot d(\mathcal{F})$$

Such a plan $(\mathcal{F}, b'(\cdot))$ can be found in O(|V|) time.

PROOF. The proof follows from Lemma 4.1, which uses algorithm Fix-charge to implement the argument used in Lemma 4.1 to find a feasible fight mission plan.

Theorem 4.4. The flight plan $(\mathcal{F}, b'(\cdot))$ returned by algorithm Find-plan [V, d] has cost

$$\tau(\mathcal{F}) + \tau_c(b(\mathcal{F})) = O(\mathsf{OPT}_{\mathsf{DFP}}) + O(1).$$

PROOF. Let $(\mathcal{F}^*, b^*(\cdot))$ be an optimal flight plan for (DFP). Clearly, this plan can be trivially turned into a feasible solution (\mathcal{F}^*, x) for (SDFP) by setting $x_k = \overline{B}$ for all $\mathcal{F}_k \in C$. It follows that

$$\mathsf{OPT}_{\mathsf{SDFP}} \le \widehat{d}(\mathcal{F}^*). \tag{17}$$

On the other hand, Lemma 4.3 implies that

$$\widehat{d}(\mathcal{F}) \le \frac{3}{2} \left(\frac{1+\alpha}{1-\alpha} \right) \mathsf{OPT}_{\mathsf{SDFP}}.$$
 (18)

Lemma 4.1 also implies that

$$\mathsf{OPT}_{\mathsf{DFP}} \ge c \cdot d(\mathcal{F}^*) + c', \tag{19}$$

while Lemma 4.2 implies that

$$b(\mathcal{F}) \le \frac{\underline{B} - x_0}{\eta_c} + \frac{\overline{c}_f \eta_d}{\eta_c} d(\mathcal{F}), \tag{20}$$

and the definition of $\widehat{d}(\cdot,\cdot)$ implies

$$\underline{c}_f d(\mathcal{F}) \le \widehat{d}(\mathcal{F}) \text{ and } \widehat{d}(\mathcal{F}^*) \le \overline{c}_f d(\mathcal{F}^*).$$
 (21)

, Vol. 1, No. 1, Article 1. Publication date: January 2017.

Putting together (17), (18), (19), (20), and (21), we obtain

$$\begin{split} &\tau(\mathcal{F}) + \tau_{\mathbf{c}}(b(\mathcal{F})) = c_{a}d(\mathcal{F}) + c_{b}b(\mathcal{F}) \\ &\leq \left(c_{a} + \overline{c}_{f}c_{b}\frac{\eta_{\mathbf{d}}}{\eta_{\mathbf{c}}}\right)d(\mathcal{F}) + c_{b}\frac{\underline{B} - x_{0}}{\eta_{\mathbf{c}}} \\ &\leq \frac{3}{2}\left(\frac{1+\alpha}{1-\alpha}\right)\frac{\overline{c}_{f}}{\underline{c}_{f}}\left(c_{a} + \overline{c}_{f}c_{b}\frac{\eta_{\mathbf{d}}}{\eta_{\mathbf{c}}}\right)\left(\frac{\mathsf{OPT}_{\mathsf{DFP}} - c'}{\underline{c}}\right) + c_{b}\frac{\underline{B} - x_{0}}{\eta_{\mathbf{c}}}. \end{split}$$

REFERENCES

- [1] 3DR Solo. 2017. https://3dr.com/solo-drone/specs/. (2017). [Online; accessed 19-Sept-2017].
- [2] BBC. 2016. How wireless power charging could recharge a flying drone. http://www.bbc.com/news/ technology-37821459
- [3] S. Bouabdallah, A. Noth, and R. Siegwart. 2004. PID vs LQ control techniques applied to an indoor micro quadrotor. In *International Conference on Intelligent Robots and Systems (IROS)*.
- [4] Endri Bregu, Nicola Casamassima, Luca Mottola, and Kamin Whitehouse. 2016. Reactive Control of Autonomous Drones. In ACM Mobile Systems, Applications, and Services (Mobisys).
- [5] Alesaandn Cappiello, Ismail Chabini, Edward K. Nam, Alessandro Lue, and Maya Abou Zed. 2002. A Statistical Model of Vehicle Emissions and Fuel Consumption. In IEEE Intelligent Transportation Systems Conf.
- [6] Chi-Kin Chau, Khaled Elbassioni, and Chien-Ming Tseng. 2017. Drive Mode Optimization and Tour Planning for Plug-in Hybrid Electric Vehicles. to be published in IEEE Trans. Intell. Transp. Syst. (2017).
- [7] Nicos Christofides. 1976. Worst-case analysis of a new heuristic for the travelling salesman problem. Technical Report. CMU. Report 388, Graduate School of Industrial Administration.
- [8] DJI Matrice 100. 2017. https://www.dji.com/matrice100/info. (2017). [Online; accessed 19-Sept-2017].
- [9] Raghu K Ganti, Nam Pham, Hossein Ahmadi, Saurabh Nangia, and Tarek F Abdelzaher. 2010. GreenGPS: a participatory sensing fuel-efficient maps application. In ACM Mobile Systems, Applications, and Services (Mobisys).
- [10] Stefan Grubwinkler and Markus Lienkamp. 2013. A modular and dynamic approach to predict the energy consumption of electric vehicles. In Conf. Future Automotive Technology.
- [11] Helicopter Flying Handbook. 2012. . US Federal Aviation Administration.
- [12] Tianxi Ji, Siheng Chen, Rohan Varma, and Jelena Kovacevic. 2015. Energy-efficient route planning for autonomous aerial vehicles based on graph signal recovery. In *Annual Allerton Conference on Communication, Control, and Computing*.
- [13] The Wall Street Journal. 2016. Amazon's Newest Ambition: Competing Directly With UPS and FedEx. http://www.wsj. com/articles/amazons-newest-ambitioncompeting-directly-with-ups-and-fedex-1474994758
- [14] Majid Khonji, Mohammed Alshehhi, Chien-Ming Tseng, and Chi-Kin Chau. 2017. Autonomous Inductive Charging System for Battery-operated Electric Drones. In ACM Workshop on Electric Vehicle Systems, Data and Applications (EV-Sys).
- [15] Samir Khuller, Azarakhsh Malekian, , and Julin Mestre. 2011. To fill or not to fill: The gas station problem. ACM Transactions on Algorithm 7 (2011), 534–545.
- [16] Eugene Kim, Jinkyu Lee, and Kang G. Shin. 2013. Real-time prediction of battery power requirements for electric vehicles. In IEEE/ACM Intl. Conf. on Cyber-Physical Systems.
- [17] Mingsong Lv, Nan Guan, Ye Ma, Dong Ji, Erwin Knippel, Xue Liu, and Wang Yi. 2016. Speed Planning for Solar-Powered Electric Vehicles. In ACM Intl. Conf. on Future Energy Systems (e-Energy).
- [18] Kenzo Nonami, Farid Kendoul, Satoshi Suzuki, Wei Wang, and Daisuke Nakazawa (Eds.). 2010. Autonomous Flying Robots: Unmanned Aerial Vehicles and Micro Aerial Vehicles. Springer Publisher.
- [19] Yasmina Bestaoui Sebbane (Ed.). 2015. Smart Autonomous Aircraft: Flight Control and Planning for UAV. CRC Press.
- [20] Roland Siegwart, Illah Nourbakhsh, and Davide Scaramuzza. 2015. Introduction to Autonomous Mobile Robots. MIT Press.
- [21] Chien-Ming Tseng and Chi-Kin Chau. 2017. Personalized Prediction of Vehicle Energy Consumption based on Participatory Sensing. to be published in IEEE Trans. Intell. Transp. Syst. (2017).
- [22] Chien-Ming Tseng, Chi-Kin Chau, Sohan Dsouza, and Erik Wilhelm. 2015. A Participatory Sensing Approach for Personalized Distance-to-Empty Prediction and Green Telematics. In ACM Intl. Conf. Future Energy Systems (e-Energy).